Prediction of impact-induced delamination in cross-ply composite laminates using cohesive interface elements

F. Aymerich, F. Dore, P. Priolo

Prediction of impact-induced delamination in cross-ply composite laminates using cohesive interface elements

F. Aymerich, F. Dore, P. Priolo

PII: S0266-3538(07)00265-5
DOI: 10.1016/j.compscitech.2007.06.015
Reference: CSTE 3756

To appear in: *Composites Science and Technology*

Received Date: 1 May 2007
Revised Date: 18 June 2007
Accepted Date: 20 June 2007

Please cite this article as: Aymerich, F., Dore, F., Priolo, P., Prediction of impact-induced delamination in cross-ply composite laminates using cohesive interface elements, *Composites Science and Technology* (2007), doi: 10.1016/j.compscitech.2007.06.015

PREDICTION OF IMPACT-INDUCED DELAMINATION IN CROSS-PLY COMPOSITE LAMINATES USING COHESIVE INTERFACE ELEMENTS

F. Aymerich, F. Dore and P. Priolo
Dipartimento di Ingegneria Meccanica - Università di Cagliari
Piazza d'Armi, 1 – 09123 Cagliari (Italy)

Abstract

The paper investigates the potential of cohesive interface elements for damage prediction in laminates subjected to low-velocity impact. FE models with interface elements adopting a bilinear cohesive law were first calibrated and validated by simulation of standard fracture toughness tests and then employed to model the impact response of cross-ply graphite/epoxy laminated plates.

The developed model provided a correct simulation of the impact response of laminates in a wide range of energy values and successfully predicted size, shape and location of main damage mechanisms. The results of the analyses also pointed out the importance of employing a damage criterion capable of accounting for the constraining effect of out-of-plane compression on the initiation of the decohesion phase.

Keywords: B. Impact behaviour, C. Delamination, C. Computational simulation

1. INTRODUCTION

Delamination is a typical interlaminar failure mode of laminated composite materials that may arise, due to the low resistance of the thin resin-rich interface existing between adjacent layers, under the action of impacts, transversal loads or free-edge stresses. This form of damage is of particular concern in primary compression-loaded structures, since internal delaminations may result in dramatic reductions in compressive strength, even when undetectable by visual inspection of the laminate surface.

The mechanics of delamination has been largely studied in the last decades by procedures that employ fracture mechanics parameters and tools [1]. The virtual crack closure technique (VCCT) [2], which is possibly the most adopted fracture mechanics tool to simulate the propagation of delamination, is based on the assumption of a pre-existing crack in the material and on the hypothesis that the strain energy released during

crack growth equals the work required to close the crack surface. The VCCT scheme suffers however from several limitations, such as a marked sensitivity to mesh density, the need of knowing in advance the size and the shape of the existing delamination, and the necessity, in most practical cases, of applying adaptive mesh regeneration strategies in order to follow the changing shape of the delamination front.

In recent years, a growing interest has emerged in the application of cohesive zone models to study delamination fractures in composite materials [1, 3-6]. Cohesive damage models presume the presence, in front of the physical crack tip, of a process zone delimited by cohesive surfaces that are held together by cohesive tractions. The cohesive tractions are related to the relative displacements of the cohesive surfaces by a constitutive law that simulates the accumulation of damage through progressive decohesion in the process zone.

The use of finite elements based on a cohesive damage approach allows to overcome the main limitations of crack closure schemes. In particular, the initiation and progression of damage are explicitly incorporated in the formulation of the element and do not necessitate external node release routines, while requirements on mesh geometry and mesh density are less stringent than those associated with crack closure techniques [7]. The main disadvantages of finite element (FE) models adopting cohesive elements are related to possible difficulties in obtaining convergence of the solution [8], and to the open problem of the identification of interface parameters required by the cohesive constitutive law [9].

The majority of studies conducted to date to analyze delamination mechanics with the use of cohesive interface elements focus on the simulation of standard interlaminar fracture toughness tests, such as double cantilever beam (DCB), end notch flexure (ENF) and mixed mode bending (MMB) [3-9]. On the other hand, because of the greater

damage complexity, only a limited number of studies are available on the prediction of the damage induced by transverse impact on laminated plates [10-15].

This paper examines the potential of surface elements based on a cohesive zone approach for damage prediction in laminates subjected to low-velocity impact. FE models with interface elements were first calibrated and validated by simulation of simple fracture mechanics tests and subsequently employed to predict the impact response of cross-ply graphite/epoxy laminates. The results of the numerical analyses were finally compared to experimental data collected during previous investigations.

2. CALIBRATION AND VALIDATION OF COHESIVE ZONE MODELS.

2.1 Cohesive element formulation and FE models

The influence of the parameters defining, for each fracture mode, the traction-separation law of interface elements and the effect of mesh density on the simulated response of DCB and ENF tests were investigated during the first phase of the study.

The analyses were carried out with the explicit solver of the commercial FE software ABAQUS 6.5, and the cohesive behaviour was incorporated in the formulation of the interface elements by a user-written material subroutine (VUMAT).

A two-parameter bilinear cohesive law was used in the study to describe the interfacial behaviour under both mode I and mode II loadings. The cohesive law relates the traction to the relative displacement between the upper and lower cohesive surfaces. The adopted mode I and mode II/III traction-separation laws consist of an initial linear elastic phase, followed by a linear softening stage that simulates the decohesion of the interface after damage initiation. The area under each traction-separation curve is assumed to equal the corresponding critical energy release rate. Complete fracture of the interface occurs when cohesive tractions vanish at the end of the decohesion stage.

Unloading occurring after damage onset is assumed to follow a linear path directly towards the origin. The original normal stiffness of the interface is however retained, even in the presence of completely degraded interfaces, under compressive loadings in order to prevent interpenetration of adjacent sublaminates at a delaminated interface.

The stress-based quadratic criterion proposed by Hou and co-workers [16] , which was developed to account for the delaying effect of compressive stresses on delamination initiation and specifically verified by experimental results for low-velocity impact, was used to assess the beginning of the decohesion stage.

According to the Hou criterion, the initiation of interface damage is controlled by the following equalities

$$\begin{aligned}
&\left(\frac{t_n}{N}\right)^2+\left(\frac{t_s}{S}\right)^2+\left(\frac{t_t}{S}\right)^2=1 && \text{for } t_n \geq 0\\
&\left(\frac{t_s}{S}\right)^2+\left(\frac{t_t}{S}\right)^2-8\cdot\left(\frac{t_n}{S}\right)^2=1 && \text{for } -\sqrt{\frac{t_s^{\,2}+t_t^{\,2}}{8}} \leq t_n < 0\\
&\textit{NO DELAMINATION} && \text{for } t_n < -\sqrt{\frac{t_s^{\,2}+t_t^{\,2}}{8}}
\end{aligned} \tag{1}$$

where t_n, t_s, t_t represent the interface stresses and N, S, T=S are the interface strengths under modes I, II and III, respectively.

The progression of damage is monitored by the scalar damage indicator d, which ranges from the initial value of 0 for the undamaged interface to the value of 1, which indicates the complete decohesion of the interface and the physical separation of the upper and lower cohesive surfaces. The evolution of the variable d is controlled by the energy dissipated as work of separation during the decohesion process.

The dependence of the fracture energy on the mode mixity is defined by the following linear interaction criterion [17]:

$$\left\{\frac{G_I}{G_{IC}}\right\}+\left\{\frac{G_{II}}{G_{IIC}}\right\}+\left\{\frac{G_{III}}{G_{IIIC}}\right\}=1 \tag{2}$$

The solution of the equilibrium equations by an explicit direct integration method requires the adoption of a time increment smaller than the critical time-step (which decreases with increasing mesh density and material stiffness and with decreasing material mass density [18]) in order to ensure the stability of the iterative time-stepping scheme. The size of the time increment requires special consideration, since an excessively small time-step may render the analysis of a dynamic event extremely intensive in terms of computing time if the total time-span of the phenomenon is many orders of magnitude larger than the time interval adopted for temporal integration.
It should also be observed that, since elements with reduced integration were employed in the present study, stabilization techniques were applied to reduce hourglassing so as to avoid excessive distortion of elements or structure [18,19].

Bidimensional FE models using 4-node plane-strain elements (CPE4R) for the composite arms and 4-node cohesive elements (COH2D4) for the midplane interface were first constructed for the analysis of DCB and ENF tests on unidirectional 18-ply graphite/epoxy laminates. Geometric nonlinearity was assumed for all FE models and contact pair surfaces were introduced when necessary (i.e. in ENF tests), in order to avoid interpenetration of sublaminates at the pre-cracked interface. The specimens were 20 mm wide and 150 mm long, with a total thickness of 3 mm and an initial crack of 35 mm. The elastic and fracture properties of the material are reported in Table 1.

The results obtained with 2D models were subsequently compared with those found with the use of 3D models created with 8-node elements (C3D8R for the composite arms and COH3D8 for the interface). In all cases investigated, the results of 2D simulations were practically coincident with those obtained by 3D models on the symmetry plane of the laminate.

Preliminary FE analyses conducted with the use of multiple (up to 12) elements across the thickness of the laminate indicated that meshes with only one element through

the height of each specimen arm, together with the adoption of the enhanced hourglass control implemented in ABAQUS, provide results that are essentially equivalent to those achieved with the use of more refined meshes.

Both mass scaling and increased loading rates were applied to the models in order to reduce the computational cost of the analysis. An appropriate displacement law with an average rate of about 10 mm/s was prescribed at nodes of load application, while density values of $1.6 \cdot 10^8$ kg/m^3 ed $1.6 \cdot 10^6$ kg/m^3 (as compared to an approximate density of $1.6 \cdot 10^3$ kg/m^3 for both graphite/epoxy laminate and pure epoxy resin) were assigned respectively to cohesive elements and to plane or solid elements modelling the composite layers. The selection of these values was guided by a series of exploratory investigations that were conducted to ensure that the modifications of mass densities and loading rates did not significantly affect the dynamic response of the models. The assigned density values, in particular, were chosen after ensuring that no significant differences existed between results of numerical simulations carried out with and without mass scaling for a reduced set of reference test cases.

2.2 Influence of cohesive parameters and mesh density

A parametric analysis was carried out in order to assess the influence of the initial stiffness and interface strength values on the response of the model.

Plots of force-displacement curves obtained with different values of the initial stiffness (fig. 1) indicate that, as already observed in previous studies [5,7], the simulated response of the laminates appears to be practically insensitive to the value of the interface stiffness. FE results reported in fig. 1 were obtained with cohesive strengths and element lengths equal, respectively, to 20 MPa and 0.28 mm for DCB tests, and to 40 MPa and 0.67 mm for ENF tests. A thickness of 20 μm, which was maintained throughout the study, was assumed for the cohesive interface. It is worth noting that the

values k_N = 120 GPa/mm and k_S = 43 GPa/mm correspond to interface stiffnesses obtained as the ratios between the elastic moduli assumed for the resin-rich layer (E = 2.4 GPa and G = 0.86 GPa) and the thickness of the interface.

An example of the influence exerted by the cohesive strength on the model response is illustrated in the graphs of fig. 2, which clearly show that the cohesive strength has a significant effect on both the peak load and the amount of stiffness reduction occurring before reaching the peak load. Interface stiffness values of 120 GPa/mm (DCB) and 43 GPa/mm (ENF), together with meshes having elements 0.1 mm (DCB) and 0.5 mm (DCB) in length, were used in the FE analyses.

Similarly to what described in previous published work [3,7,8,13], the analyses conducted during the study demonstrated that the elements size is a key factor for the development of accurate FE models. In particular, as visible in fig. 3, it was observed that the decohesion process zone ahead of the crack tip should be represented by a sufficient number of cohesive elements in order to achieve a smooth crack growth and a structural response unaffected by large oscillations and abrupt jumps or irregularities.

Figs. 4a and 4b show a comparison between predicted and experimental force-displacement curves of DCB and ENF tests on unidirectional graphite/epoxy laminates whose properties are summarized in Table 1. The values of N = 30 MPa and S = 80 MPa, which provided a good match between simulations and experiments, were employed in the FE model for normal and shear cohesive strengths, respectively. As a final example, the capability of the model to correctly predict the initiation and propagation of delamination under mixed-mode loading is illustrated in fig. 4c, which compares numerical simulations with experimental results of MMB tests carried out on unidirectional AS4/PEEK laminates by Camanho and co-workers [6].

3. MODELLING OF IMPACT DAMAGE

The information acquired during the preliminary calibration phase has been subsequently used to guide the development of an FE model that simulates the low-velocity impact behaviour of composite laminates.

The model predictions were validated by comparison with experimental data collected during the course of a previous study on the damage response of impacted $[0_3/90_3]_S$ cross-ply laminates of the same graphite/epoxy material analyzed in the preceding paragraph. Experimental observations [20] showed that initial damage consists of a tensile crack in the distal 0º layers, followed by shear matrix cracks and by delaminations developing, with a typical two-lobe shape, on the lower 90º/0º interface. Starting from impact energy levels of about 5 J, localized matrix crushing takes place underneath the contact area, while small delaminations initiate on the top 0º/90º interface at impact energies of approximately 7 J. Fibre fracture is observed only for impacts with energies higher than 8 J.

The composite specimens (65 mm × 87.5 mm in size) were simply supported by a steel plate having a rectangular opening 45 mm × 67.5 mm in size, and impacted by a 2.3 kg mass having a hemispherical indenter of 12.5 mm in diameter. Because of symmetry, only one quarter of the model was built and analysed. $0°_3$ and $90°_3$ sublaminates were modelled through their thickness with two C3D8R reduced integration solid elements, while COH3D8 cohesive elements were inserted at the two interfaces between layers with different orientation (top 0°/90° interface and bottom 90°/0° interface). Vertical interface elements were also placed on the symmetry plane parallel to the 0° direction to simulate the growth of the tensile matrix crack in the 0º layers. An element size of 0.25 mm by 0.25 mm (on the laminate plane) was used in the highest density region of the mesh. No mass scaling was used in the model.

Impacts of different energies were simulated by imposing to the impactor (modelled as a rigid body with an assigned mass of 2.3/4 kg) the appropriate velocities at the instant of contact. The interaction between the plate and the indentor was simulated by surface-to-surface contact elements connecting the indenter and laminate surfaces.

Calculations were performed on a distributed-memory cluster system of five Linux workstations equipped with a dual-core 3.4 GHz x-86 processor and interconnected with Gigabit Ethernet, using the MPI-based parallel solver available in ABAQUS/Explicit.

The elastic and interlaminar fracture properties reported in Table 1 were used in the analysis and the value of mode II fracture energy was adopted for mode III toughness.

On the basis of the indications gathered during the calibration phase, the following values were assigned to initial stiffnesses and cohesive strengths of the interface:

k_N = 120 GPa/mm; $k_S = k_T$ = 48 GPa/mm

N = 30 MPa; $S = T$ = 80 MPa.

Fig. 5 shows that a very good agreement is observed between experiments and predictions in both the peak force values and the impact durations for impact energies up to about 5 J. The difference observed, especially in maximum force values, beyond this level may be attributed to the onset of major damage phenomena, such as matrix crushing around the contact region, not accounted for in the simulation.

A reasonably good agreement was also observed between simulated and experimental results in terms of damage evolution and delamination size. Numerical analyses indicate that the initial damage, occurring at a load level about 500 N, consists of a tensile matrix crack that develops within the distal stack of 0° plies and quickly propagates towards the boundary of the sample. Following the formation of this crack, and in accordance with experimental evidence, the model predicts the onset of delamination on the lower 90°/0° interface and its growth with the characteristic two lobed shape elongated along the 0° direction (figs. 6, 7). The development of minor delaminations on the upper 0°/90°

interface at an impact energy level of approximately 7 J is also correctly simulated by the numerical model, as illustrated in fig. 8. The growth rate of the delamination on the lower 90°/0° interface with increasing impact energy is successfully predicted by the FE model, as visible in Fig. 9, which shows a comparison of delamination lengths and delamination widths obtained numerically and experimentally in the range of impact energies investigated.

As a final remark, it should be noticed that the results obtained by the FE model highlighted the importance of adopting a criterion able to account for the constraining effect of out-of-plane compression on the initiation of the decohesion phase. This point is made evident by the largely inaccurate predictions of extensive delaminations at the upper 0°/90° interface (fig. 10) that are provided by the model -even for impact energies as low as 2 J- when adopting the following damage criterion:

$$\left(\frac{\langle t_n \rangle}{N}\right)^2 + \left(\frac{t_s}{S}\right)^2 + \left(\frac{t_t}{S}\right)^2 = 1 \qquad (3)$$

which neglects the delaying action exerted by through-thickness compressive stresses on delamination onset.

CONCLUSIONS

The potential of interface elements based on a bilinear cohesive failure model for damage prediction in laminated composites subjected to low-velocity impact has been investigated in the paper.

The developed FE model provided a correct prediction of the impact response of laminates in a wide range of impact energy values and successfully simulated the sequence and location of damage mechanisms. Very good agreement was also achieved between numerical predictions and experimental observations in terms of shapes, orientations and sizes of delaminations induced by impact. The results of the FE analyses

also showed the necessity of adopting a damage onset criterion capable of accounting for the constraining effect of out-of-plane compression on the initiation of the decohesion phase.

ACKNOWLEDGEMENTS

This work was supported by MIUR - Italian Ministry of University and Scientific and Technological Research (*CyberSar* project) and by ENEA - Italian National Agency for New Technologies, Energy and the Environment (*Promomat* project).

References

[1] Tay TE. Characterization and analysis of delamination fracture in composites: An overview of developments from 1990 to 2001. Applied Mechanics Review 2003; 56(1): 1-32.
[2] Krueger R. Virtual crack closure technique: History, approach, and applications. Applied Mechanics Review 2004; 57(2): 109-143.
[3] Mi Y, Crisfield MA, Davies GAO, Hellweg HB. Progressive delamination using interface elements. Journal of Composite Materials 1998; 32(14): 1246-1273.
[4] Borg R, Nilsson L, Simonsson K. Modeling of delamination using a discretized cohesive zone and damage formulation. Composites Science and Technology 2002; 62: 1299-1314.
[5] Zou Z, Reid SR, Li S. A continuum damage model for delaminations in laminated composites. Journal of the Mechanics And Physics of Solids 2003; 51: 333-356.
[6] Camanho PP, Davila CG, De Moura MF. Numerical simulation of mixed-mode progressive delamination in composite materials. Journal of Composite Materials 2003; 37(16): 1415-1438.
[7] Turon A, Dávila CG, Camanho PP, Costa J. An engineering solution for mesh size effects in the simulation of delamination using cohesive zone models. Engineering Fracture Mechanics 2007; 74(10): 1665-1682.
[8] Alfano G, Crisfield MA. Finite element interface models for the delamination analysis of laminated composites: mechanical and computational issues. International Journal for Numerical Methods in Engineering 2001; 50(7): 1701-1736.
[9] Corigliano A, Mariani S. Simulation of damage in composites by means of interface models: parameter identification. Composites Science and Technology 2001; 61: 2299-2315.
[10] Wisheart M, Richardson MOW. The finite element analysis of impact induced delamination in composite materials using a novel interface element. Composites part A: Applied science and manufacturing 1998; 29: 301-313.
[11] de Moura MFSF, Gonçalves JPM. Modelling the interaction between matrix cracking and delamination in carbon-epoxy laminates under low velocity impact. Composites Science and Technology 2004; 62: 1021-1027.
[12] Borg R, Nilsson L, Simonsson K. Simulation of low velocity impact on fiber laminates using a cohesive zone based delamination model. Composites Science and Technology 2004; 64: 279-288.
[13] Geubelle PH, Baylor JS. Impact-induced delamination of composites: a 2D simulation. Composites Part B: Engineering 1998; 29(5): 589-602.
[14] Zhang Y, Zhu P, Lai X. Finite element analysis of low-velocity impact damage in composite laminated plates. Materials and Design 2006; 27: 513-519.
[15] Nishikawa M, Okabe T, Takeda N. Numerical simulation of interlaminar damage propagation in CFRP cross-ply laminates under transverse loading. International Journal of Solids and Structures 2007; 44(10): 3101-3113.
[16] Hou JP, Petrinic N, Ruiz C. A delamination criterion for laminated composites under low-velocity impact. Composites Science and Technology 2001; 61: 2069-2074.
[17] Reeder JR. An evaluation of mixed-mode delamination failure criteria. NASA TM 104210, 1992.
[18] Belytschko T, Liu WK, Moran B. Nonlinear finite elements for continua and structures. New York, John Wiley & Sons, 2000.
[19] Abaqus Theory Manual, Version 6.5, 2004, Abaqus, Inc.

[20] Aymerich F, Pani C, Priolo P. Damage response of stitched cross-ply laminates under impact loadings. Engineering Fracture Mechanics 2007; 74(4): 500-514.

Figure captions

Fig. 1. Effect of initial interface stiffness on force-displacement curves of simulated DCB (a) and ENF (b) tests

Fig. 2. Effect of interface strength on force-displacement curves of simulated DCB (a) and ENF (b) tests

Fig. 3. Effect of mesh density on force-displacement curves of simulated DCB (a) and ENF (b) tests. The process zone is about 1.5 mm long in DCB specimens and 8 mm long in ENF specimens. The traces of the embedded graph of fig. 3a are vertically shifted for better readability.

Fig. 4. Comparison of predicted and experimental results for DCB, ENF ed MMB tests. Experimental MMB data are from Camanho et al. [6]

Fig. 5. Comparison between predicted and experimental force-time curves for impact energies ranging between 1 J and 7 J

Fig. 6. Comparison between predicted delamination and damage as observed by X-radiography

Fig. 7. Delamination areas predicted by the model under increasing impact energies

Fig. 8. Comparison between predicted delaminations and ultrasonic C-scans for a laminate impacted at 7 J.

Fig. 9. Predicted and measured delamination length and width on the bottom 90°/0° interface as a function of impact energy

Fig. 10. Delaminations predicted by the model for an impact energy of 2.1 J when neglecting the effect of out-of-plane compression in the damage onset criterion.

Tables

Table 1: Elastic and fracture properties used in simulations of DCB and ENF tests for graphite/epoxy laminates

E_{11} = 93.7 GPa; $E_{22} = E_{33}$ = 7.45 GPa
$G_{12} = G_{23} = G_{13}$ = 3.97 GPa
$\nu_{12} = \nu_{23} = \nu_{13}$ = 0.261
G_{Ic} = 520 J/m^2; G_{IIc} = 970 J/m^2

Fig.1

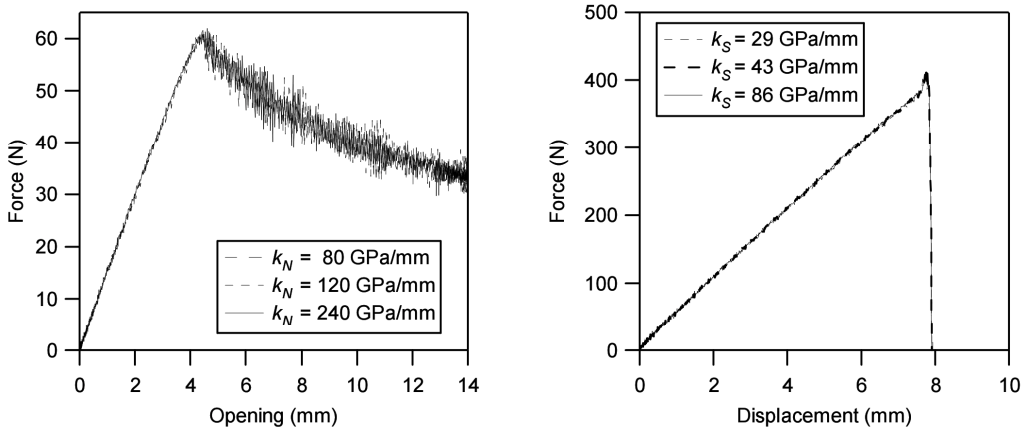
Force (N)
Opening (mm)
k_N = 80 GPa/mm
k_N = 120 GPa/mm
k_N = 240 GPa/mm
(a)
Force (N)
Displacement (mm)
k_S = 29 GPa/mm
k_S = 43 GPa/mm
k_S = 86 GPa/mm
(b)

Fig.2

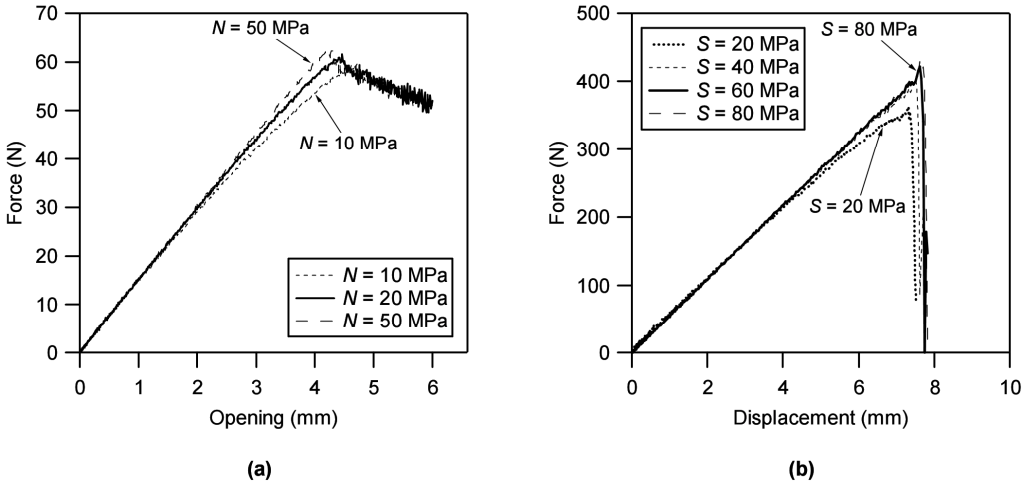
Force (N)
Opening (mm)
N = 50 MPa
N = 10 MPa
N = 10 MPa
N = 20 MPa
N = 50 MPa
(a)
Force (N)
Displacement (mm)
S = 80 MPa
S = 20 MPa
S = 20 MPa
S = 40 MPa
S = 60 MPa
S = 80 MPa
(b)

Fig.3

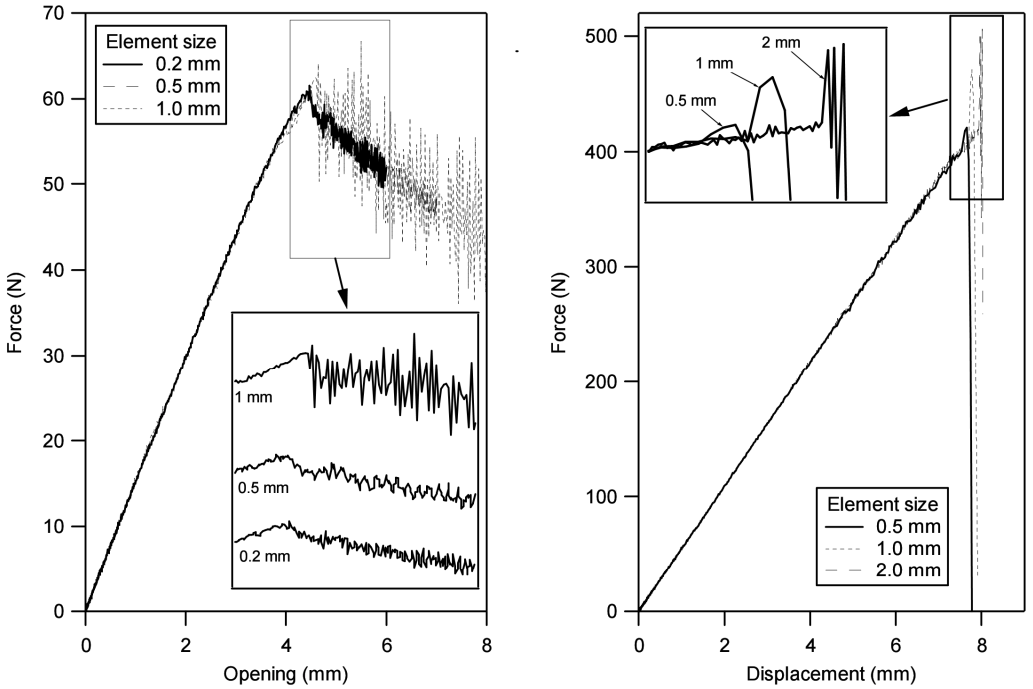

Fig.4

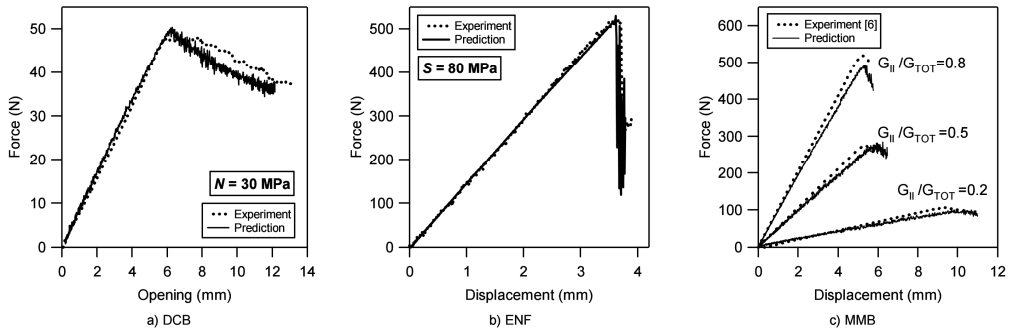

Fig.5

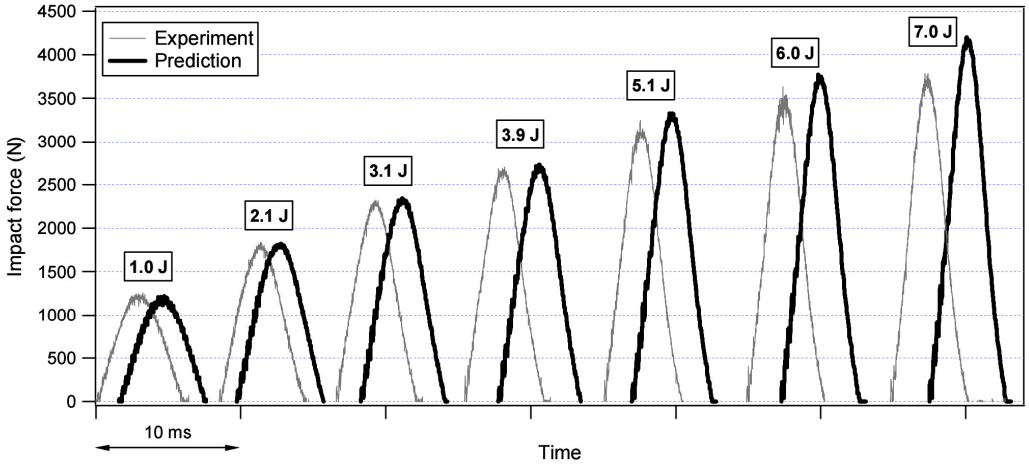

Fig.6

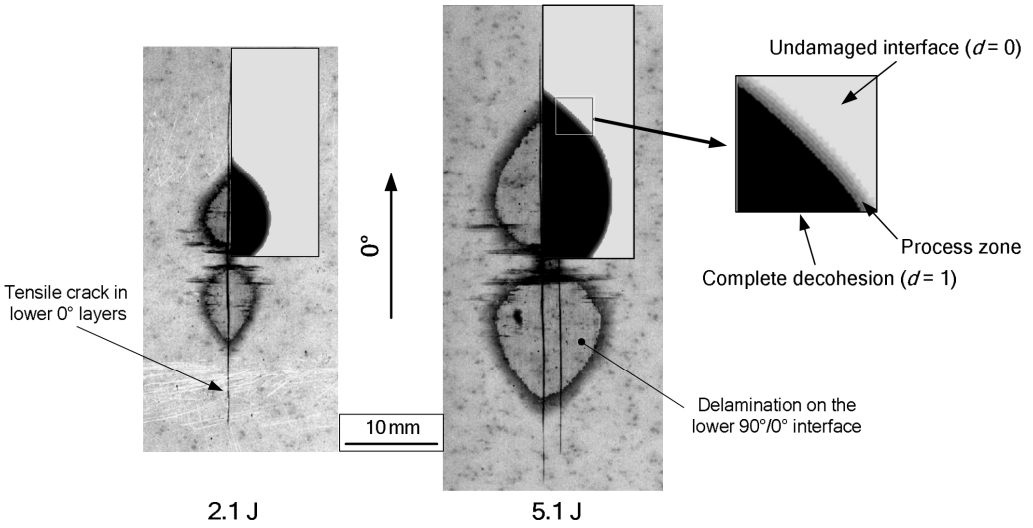

Fig.7

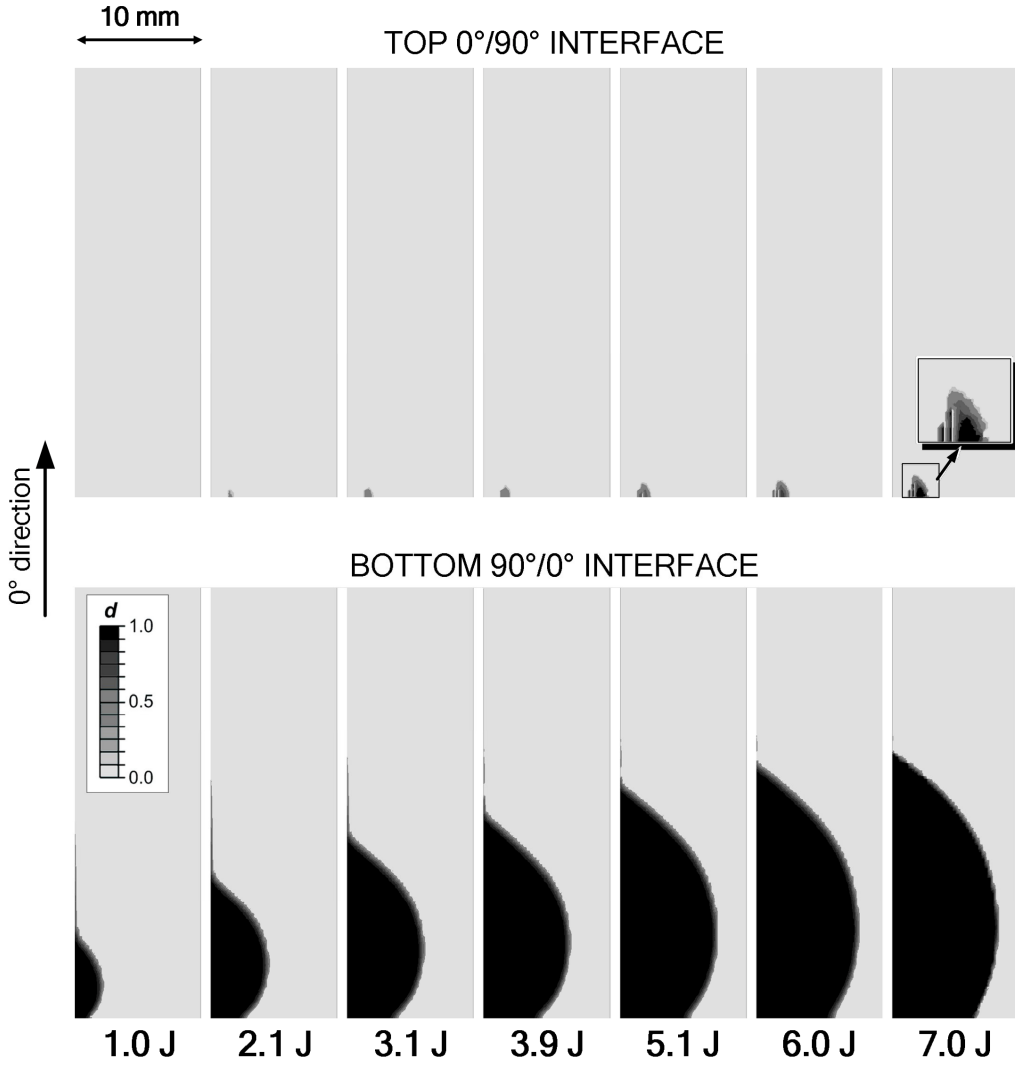
10 mm
TOP 0°/90° INTERFACE
0° direction
BOTTOM 90°/0° INTERFACE
d
1.0
0.5
0.0
1.0 J
2.1 J
3.1 J
3.9 J
5.1 J
6.0 J
7.0 J

Fig.8

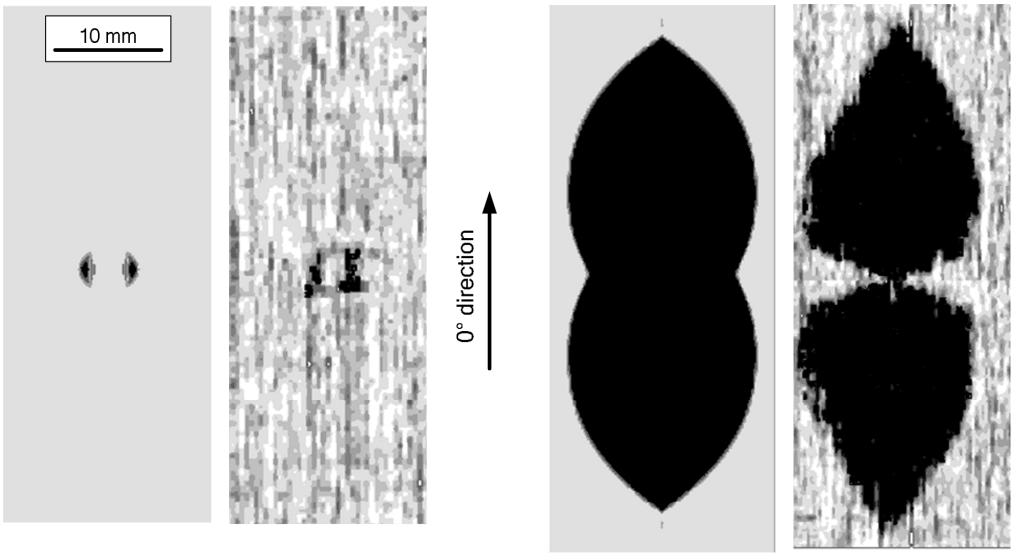

Fig.9

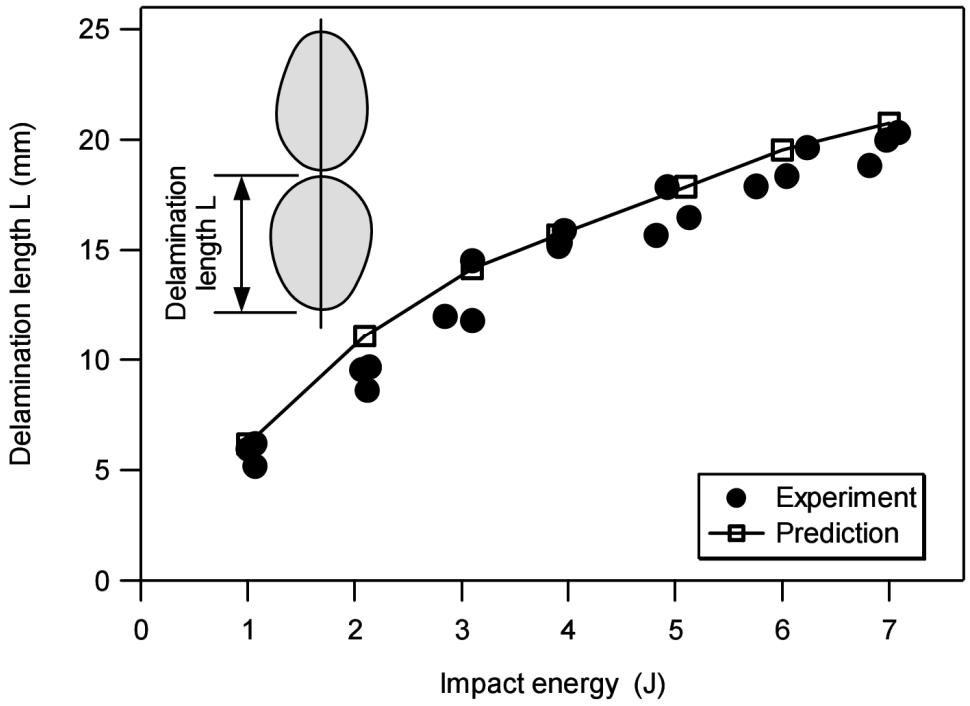

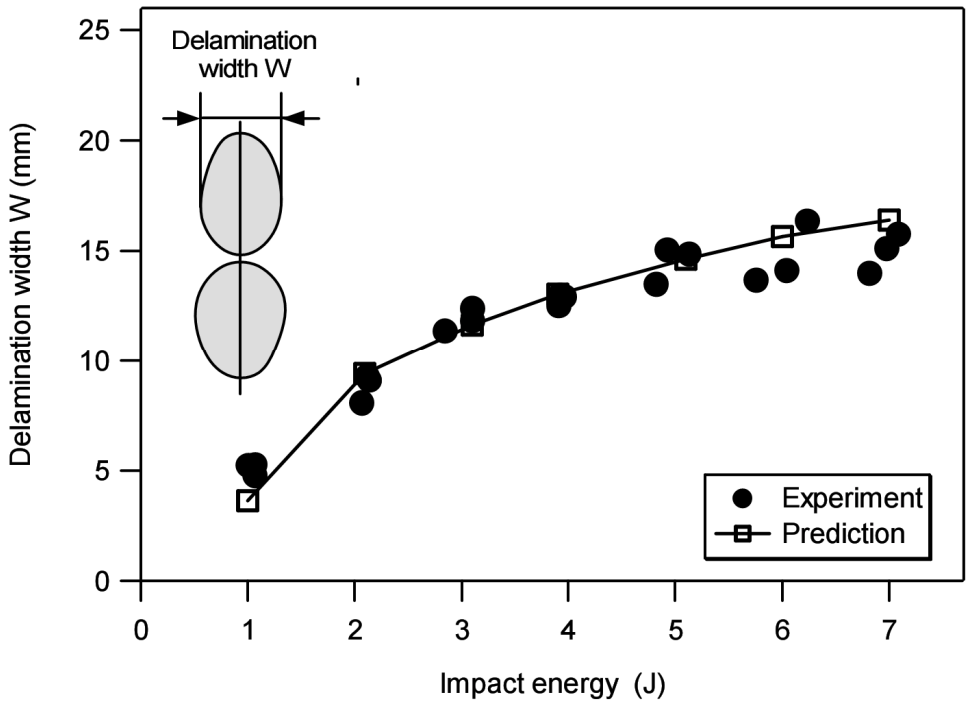

Fig.10